ACS APPLIED MATERIALS & INTERFACES

Research Article

www.acsami.org

All-Solution-Processed Inverted Quantum-Dot Light-Emitting Diodes

Alice Castan, Hyo-Min Kim, and Jin Jang*

Department of Information Display, Advanced Display Research Center, Kyung Hee University, Seoul 130-701, Korea

Supporting Information

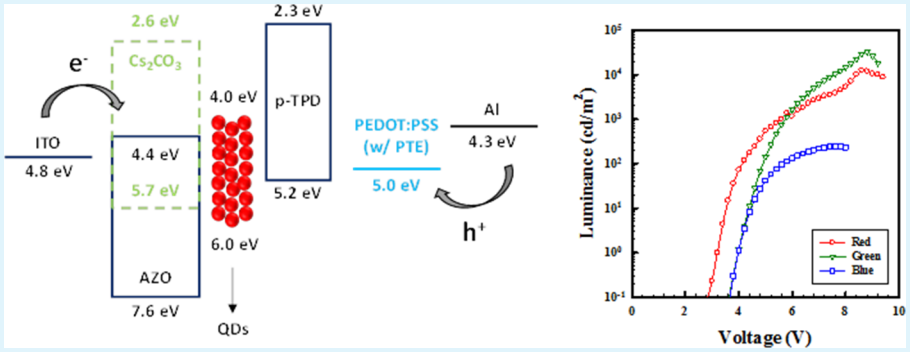

ABSTRACT: Quantum dots are a promising new candidate for the emissive material in light-emitting devices for display applications. The fabrication of such devices by solution processing allows considerable cost reduction and is therefore very attractive for industrial manufacturers. We report all solution-processed colloidal quantum-dot light-emitting diodes (QLEDs) with an inverted structure. The red, green, and blue devices showed maximum luminances of 12 510, 32 370, and 249 cd/m^2 and turn-on voltages of 2.8, 3.6, and 3.6 V, respectively. We investigate the effect of a surfactant addition in the hole injection layer (HIL), with the aim of facilitating layer deposition and thereby enhancing device performance. We demonstrate that in the device structure presented in this study, a small amount of surfactant in the HIL can significantly improve the performance of the QLED.

KEYWORDS: *all-solution-process, inverted structure, polyoxyethylene tridecyl ether, QLED, quantum dot*

1. INTRODUCTION

Colloidal quantum dots (QDs) possess unique characteristics that make them a good candidate for the emissive material in light-emitting devices. They show high color purity and high quantum yield, and their emission wavelength can be tuned by controlling the core size of the QDs during synthesis.[1] The field of quantum-dot light-emitting diodes (QLED) has therefore been expanding, and devices with increasingly high performances have been fabricated.

QLEDs with an inverted structure are very advantageous for display applications. The bottom transparent cathode can be directly connected to n-channel metal oxide or amorphous silicon based thin-film transistor (TFT) backplanes.[2,3] In recent years, high performance QLEDs with an inverted structure have been reported.[4−6] High luminance, high efficiency, and low operating voltages have been achieved, leading to a potential candidate for future display applications.

In comparison with QDs synthesized by epitaxial growth, colloidal QDs are fabricated using wet chemical methods. Colloidal QDs are therefore solution processable,[7−10] which opens up the possibility of all solution-processed QLEDs. This offers considerable advantages compared with thermal evaporation in high vacuum, which is the conventional method for device fabrication.[11] Thermal evaporation is not fit for large area applications, which is a major drawback for industrial manufacturing. Solution processing is a way to avoid this issue, and thus process cost can be reduced, and large scale fabrication is possible.[12] Being able to fabricate red, green, and blue devices using the same structure is also advantageous in terms of manufacturing throughput in display applications.

One of the inconveniences of solution processing for multilayer structures is that there is a possibility of causing damage to the underlying layer when depositing the over layer.[13,14] If the solvent used for the over layer can dissolve the underlying layer, there is a great chance of layer intermixing. This phenomenon obviously leads to decreased performance of the QLEDs, since a perfect multilayer structure cannot be obtained. Therefore, it is necessary to use orthogonal solvents for consecutive layers to prevent layer intermixing.

Another issue with using solution-based techniques such as spin-coating for device fabrication is trying to ensure good wetting of the over layer solution on top of the underlying layer. For instance, a water based solution will have very poor wetting on top of a hydrophobic thin film, which jeopardizes the layer deposition. When this problem occurs, it is difficult or impossible to control the thickness and uniformity of the layer,

Received: November 5, 2013
Accepted: January 27, 2014
Published: January 27, 2014

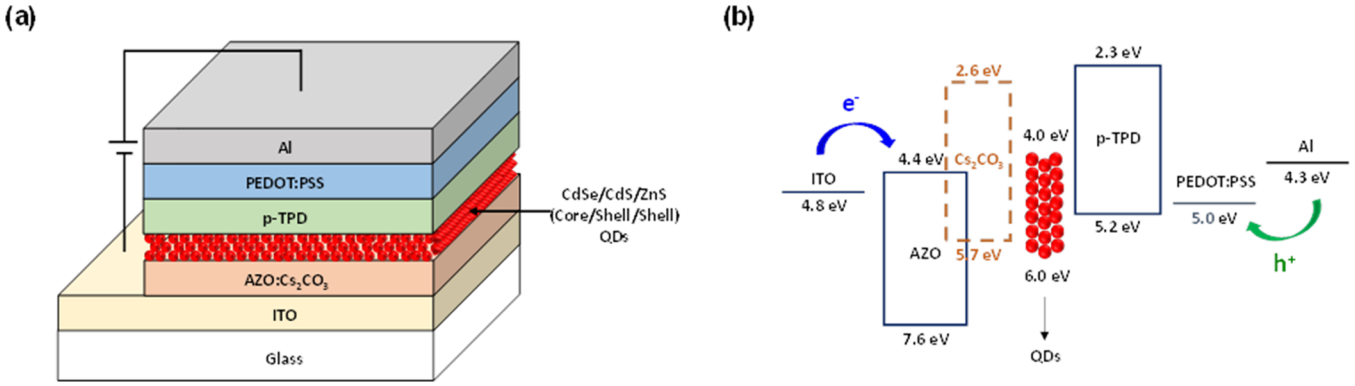

Figure 1. (a) Schematic cross-sectional view and (b) energy band diagram of the red-emitting all-solution-processed QLED with an inverted structure.

which can dramatically impair the performance of the device. To this difficulty, it is possible to add a low boiling point solvent or a surfactant in the solution to increase the wetting on the substrate. In this study, polyoxyethylene tridecyl ether (PTE), a nonionic surfactant, is used to facilitate the deposition of aqueous poly(ethylenedioxythiophene)/polystyrenesulfonate (PEDOT:PSS) on the hydrophobic polymer hole transport material for the QLEDs.

As mentioned earlier, solution processes show great advantages for industrial manufacturing. All-solution-processed QLED devices with conventional structures have already been reported.[15−17] Holloway et al.[16] reported solution-processed QLEDs using ZnO nanoparticles as the electron transport material, showing maximum luminances of 31 000, 68 000, and 4200 cd/m^2 for orange-red, green, and blue, respectively. The devices also showed promising stability, with a 270 h lifetime at a luminance of 600 cd/m^2. Recently, Choi and co-workers reported all-solution-processed inverted QLEDs using polyethylenimine ethoxylated (PEIE) as a surface modifier to reduce ITO work function.[18] Their optimized red-emitting device had maximum luminance and current efficiency of 2900 cd/m^2 and 0.35 cd/A, respectively.

In this study, we focused on the effect of various PTE concentrations in the PEDOT:PSS layer to improve layer deposition and uniformity. We verified its effect by contact angle measurement, which decreased with increasing PTE content. Nevertheless, we also found that increasing PTE concentration led to a decrease in the hole current flow. Therefore, we attempted to optimize the surfactant concentration in the layer to find a compromise between those two phenomena in the red QLED. We found that adding 0.5% PTE in volume to the solution before spin-coating led to the best device performance. This optimized PTE content was then applied for the fabrication of green and blue devices, and we obtained maximum luminances of 12 510, 32 370, and 249 cd/m^2 and turn-on voltages of 2.8, 3.6, and 3.6 V for the red, green, and blue QLEDs, respectively.

2. EXPERIMENTAL SECTION

Four red-emitting QLEDs were fabricated using the following structure: glass/indium tin oxide (ITO)/Al doped zinc oxide (AZO):cesium carbonate (Cs_2CO_3, ∼40 nm)/QDs (2.5−3.5 monolayers (MLs))/poly(4-butylphenyl-diphenyl-amine) (p-TPD, ∼25 nm)/PEDOT:PSS (∼47 nm)/Al (∼100 nm) as shown in Figure 1a; the PEDOT:PSS layers of each device contain a different amount of PTE.

To fabricate the AZO:Cs_2CO_3 layer, first, a 30% AZO solution was prepared according to the method used in ref 4. In a three necked beaker, 2.2 g of zinc acetate dehydrate ($Zn(C_4H_6O_4)\cdot 2H_2O$) was mixed with 30% aluminum hydroxide acetate ($HOAl(C_2H_3O_2)_2$), and monoethanolamine (MEA) was added to the powder to stabilize the resulting AZO complex. The complex was then dissolved in 100 mL of ethanol and refluxed for 9 h at a temperature of 80 °C, until a translucent AZO solution was obtained. We made a 20 mg/mL Cs_2CO_3 solution by adding Cs_2CO_3 powder to ethanol, and stirring for around 12 h, until complete dissolution of the powder. The AZO solution was then mixed with the 20 mg/mL solution of Cs_2CO_3, with a volume ratio of 5:1. The solution was stirred for 5 h.

In order to study the effect of the concentration of PTE in the PEDOT:PSS layer on the device performance, four different solutions were used for the fabrication of the PEDOT:PSS HILs. The first solution consisted only of deionized (DI) water based PEDOT:PSS (Clevios P VP AI 4083), and the other four were obtained by mixing PEDOT:PSS with 0.3%, 0.5%, 1.0%, and 1.5% PTE by volume. We made one device using each one of these solutions for the HIL material. In the case of the solution of PEDOT:PSS mixed 0.5% PTE, 100 μL of a 10% PTE dilution in DI water was added to 2 mL of PEDOT:PSS and stirred for over 5 h.

Two additional devices were made using the same structure as the red device (with 0.5% PTE in the PEDOT:PSS layer) but replacing the red QDs (634 nm) with green (537 nm) and blue (441 nm) QDs. The absorbance spectra and normalized photoluminescence (PL) intensities for the red, green, and blue QDs are given in Figure S1 in the Supporting Information. Figure S1 in the Supporting Information shows the good color purity of the light emitted by the QDs, with full widths at half-maximum (fwhm) of 37, 23, and 27 nm for red, green, and blue, respectively.

The ITO glass substrates were cleaned for 15 min in an ultrasonicator with acetone, methanol, and isopropyl alcohol (IPA) sequentially. They were then rinsed with DI water for 2 min and dried by N_2 blowing. Except for the Al electrode, all layers were successively spin coated on the substrates in a N_2 filled glovebox. First, the AZO:Cs_2CO_3 layer was spin coated as the electron transport layer (ETL) at 4500 rpm for 25 s and annealed at a temperature of 225 °C for 10 min in ambient air. The other layers were all annealed in the N_2 filled glovebox for 10 min. On top of the AZO:Cs_2CO_3 layer, CdSe/CdS/ZnS (core/shell/shell type) QDs dissolved in toluene at a concentration of 5 mg/mL (NanoSquare Inc., Korea) were spin coated at 1500 and 1000 rpm for the red and green QDs, respectively. In the case of the blue-emitting device, CdS/ZnS (core/shell) QDs were spin coated at 400 rpm. All QD layers were annealed at a temperature of 190 °C. A solution of 1.0 wt % p-TPD in dichlorobenzene was then deposited as the hole transport layer (HTL) at 2000 rpm for 25 s and annealed at 160 °C. Finally the PEDOT:PSS, acting as the HIL, was spin coated, adjusting the spin speed for each one of the four solutions so as to obtain the same layer thickness of around 45 nm for all the devices; the annealing temperature was set to 160 °C. A ∼100 nm

thick Al anode was deposited on top of the PEDOT:PSS by thermal evaporation in high vacuum, after which the devices were encapsulated with glass.

The current density−voltage and luminance−voltage characteristics were measured using a Konica Minolta CS100A luminance meter coupled with a Keithley 2635A voltage and current source meter. Contact angles were measured using a Phoenix 600 measurement system. Absorbance and PL of the QDs in the Supporting Information were measured with a Scinco S-4100 UV−visible spectrophotometer and Jasco FP-6500 spectrofluorometer, respectively.

3. RESULTS AND DISCUSSION

Figure 1b shows the energy band diagram of the red-emitting all-solution-processed inverted QLED fabricated in this study.

Table 1. Contact Angle Data for Various PTE Concentrations in PEDOT:PSS

PTE concentration in PEDOT:PSS (%)	contact angle (deg)	wetting energy (mN/m)	work of adhesion (mN/m)
0	79	14	87
0.5	39	57	129
1	35	59	132
1.5	32	61	134

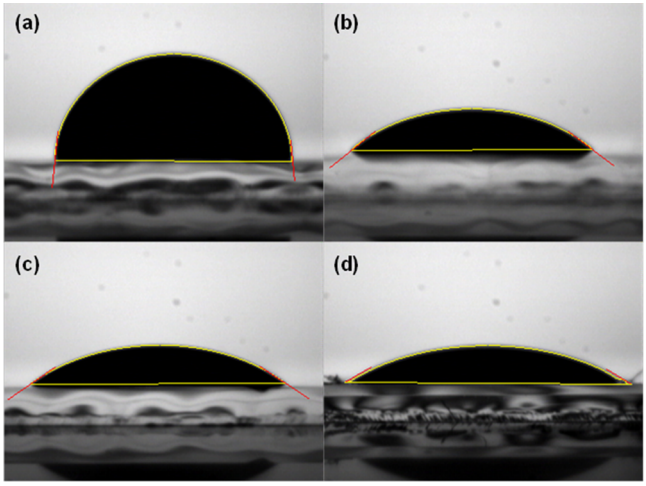

Figure 2. Contact angle images of PEDOT:PSS with various PTE concentrations: (a) 0, (b) 0.5%, (c) 1.0%, and (d) 1.5%.

Contrary to a conventional structure QLED, the electrons are injected from the ITO electrode that serves as the cathode, and the holes are injected from the Al electrode that serves as the anode. The electrons are transported through the AZO:Cs_2CO_3 ETL to the QD emissive layer (EML); and the holes are transported through the PEDOT:PSS HIL and then the p-TPD HTL. According to this energy band diagram, it can be noted that the reasonably small energy gap of ∼0.8 eV between the poly-TPD and the QD highest occupied molecular orbital (HOMO) levels makes p-TPD a good material for the transport of holes to the EML but that the efficiency of the devices could still be enhanced by using a material with a deeper HOMO energy level. However, the ∼1.7 eV difference between its lowest unoccupied molecular orbital (LUMO) level and that of the QDs makes p-TPD an excellent electron blocking material. The same observation can be made for the AZO:Cs_2CO_3 layer, whose conduction band level matches well the work function of the ITO, with a 0.4 eV energy gap, and can therefore be considered as a good choice for electron injection, while effectively preventing holes from passing through the EML because of its high valence band energy level (1.6 eV energy gap between the EML and ETL valence band energy levels).

AZO was chosen as the ETL material because of its effect on the brightness of inverted QLEDs. The effect of doping in ZnO by Al on the performance of inverted structure QLEDs has already been studied.[4] As was demonstrated in this study, adding Al in the ZnO sol−gel solution before spin coating led to a considerable increase in brightness, and the efficiency was also enhanced. The best condition for improving the performance was shown to be a concentration of 30% aluminum in AZO.

However, as it is also shown in the study, increasing Al doping concentration in the ZnO thin films has the disadvantage of increasing their resistivity. The conductivity of a 33 nm 30% AZO thin film is approximately 6 orders of magnitude lower than that of a ZnO thin film of the same thickness.[4] Therefore, we chose to use Cs_2CO_3 doped AZO as the ETL material for this experiment. Cs_2CO_3 is a known n-type dopant that has already been used to enhance charge injection in both organic[19] and inorganic[20] electron transport materials. Moreover, the improvement of the performance of inverted QLEDs by adding Cs_2CO_3 in the AZO ETL has already been demonstrated.[21] The dopant concentration was optimized prior to this study for minimizing turn-on and driving voltages. The optimized volume ratio for these criteria of 0.2 M AZO to a 20 mg/mL Cs_2CO_3 solution in ethanol was found to be 5:1.

To illustrate the effect of PTE concentration on the wetting ability of PEDOT:PSS, we measured the contact angles of the four HIL solutions (PEDOT:PSS mixed with 0, 0.5%, 1.0%, and 1.5% PTE by volume) on the p-TPD surface. The results are displayed in Table 1, and the images of the drops of PEDOT:PSS on the p-TPD surface are shown in Figure 2 for (a) 0, (b) 0.5%, (c) 1.0% and (d) 1.5% PTE.

Figure 2 clearly shows the difference in the aspect of the PEDOT:PSS drops when PTE is not added and when PTE is added. In Table 1, contact angles were determined from the results measured three times, and the wetting energy and work of adhesion values were calculated from the average contact angles. As can be observed in Table 1, adding PTE results in a decrease of the contact angle between PEDOT:PSS and p-TPD: the contact angle drops from 79° to 39° when going from 0 to 0.5% PTE and then decreases less drastically to 35° and 32° for 1.0% and 1.5% PTE, respectively. These results indicate that the wetting of the surface is improved when PTE concentration is increased. It should be noted that the very slight difference between the contact angles for PTE concentrations of 0.5−1.5% shows that adding only a small amount of PTE (0.5%) in PEDOT:PSS is sufficient to improve wetting.

In order to study the effect of adding PTE on the transport of holes in the QLEDs, hole only devices (HOD) were fabricated with the following structure: glass/ITO/PEDOT:PSS (∼45 nm)/p-TPD (∼25 nm)/PEDOT:PSS with or without PTE (∼85 nm)/Al. We chose a thicker PEDOT:PSS layer than the one used for the fabrication of the QLEDs, so as to have more visibility of the variation of the current flow in the material. Four devices were made using four solutions with various concentrations of PTE (0, 0.5%, 1.0%, and 1.5% by volume) for the ∼85 nm thick PEDOT:PSS layer.

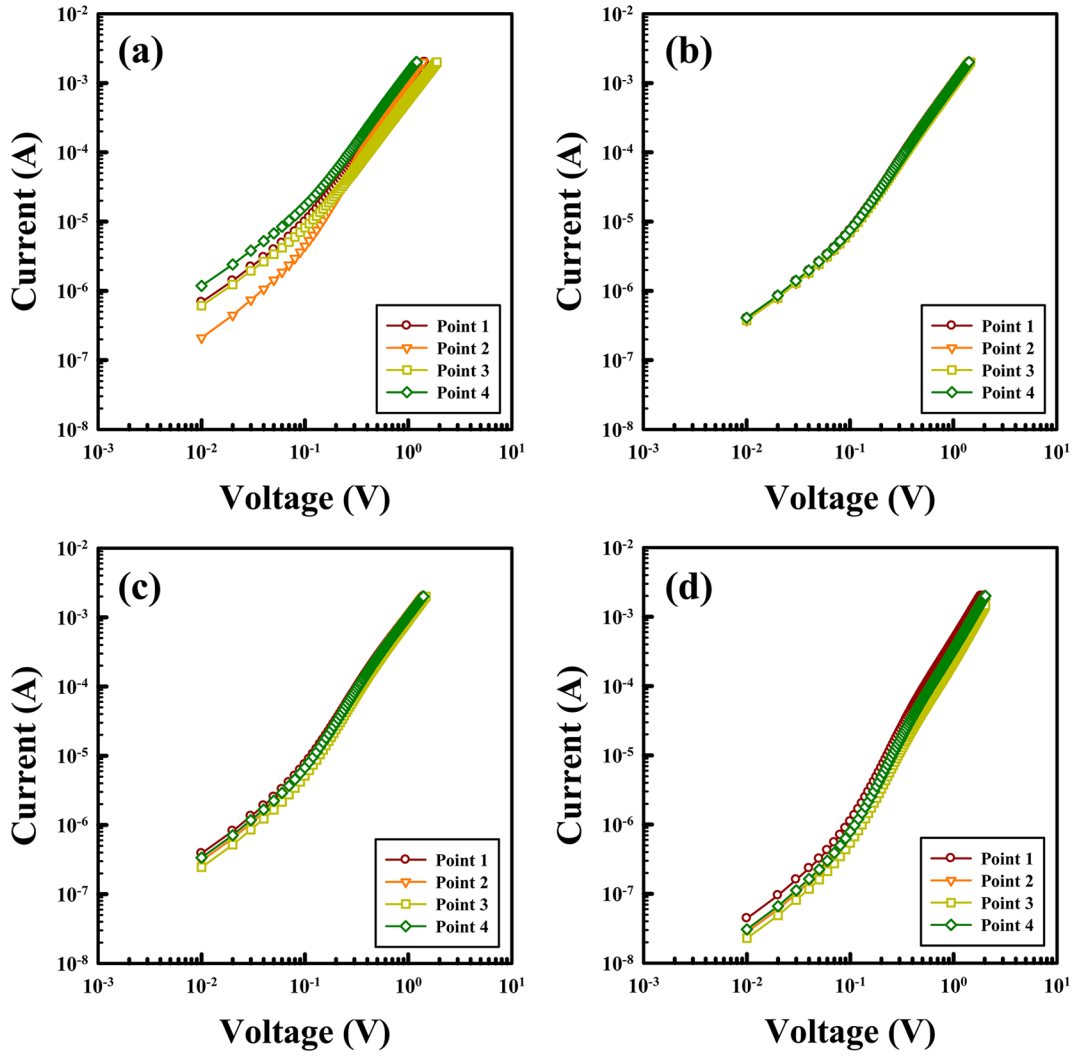

Figure 3. Current–voltage characteristics measured on four different points of the HODs (ITO/PEDOT:PSS/p-TPD/PEDOT:PSS with or without PTE/Al), with various PTE concentrations in PEDOT:PSS: (a) 0, (b) 0.5%, (c) 1.0%, and (d) 1.5%.

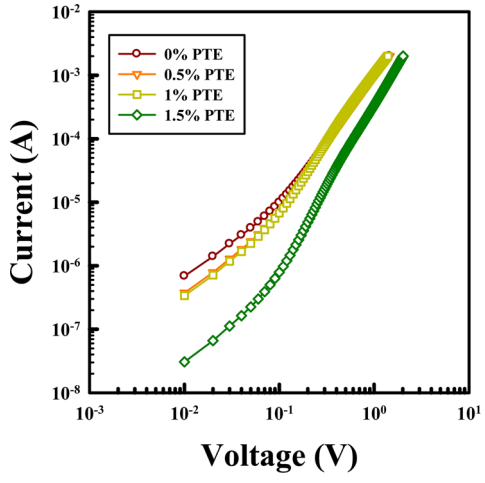

Figure 4. Current–voltage characteristic of the HODs for various PTE concentrations in PEDOT:PSS.

Figure 3 shows the log current–voltage characteristics for the four HODs with (a) 0, (b) 0.5%, (c) 1.0%, and (d) 1.5% PTE in the PEDOT:PSS layer, each measured on four different points of the devices. The uniformity of the current flow is

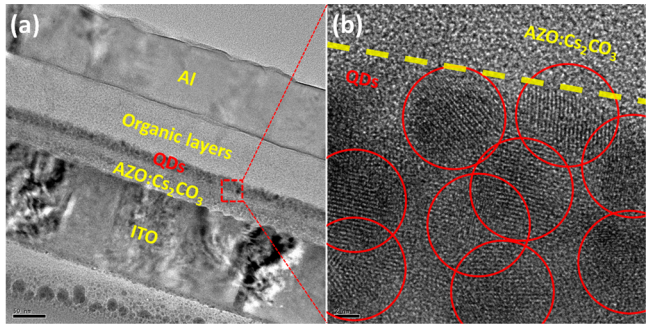

Figure 5. TEM image of the red-emitting all-solution-processed inverted QLED (ITO/AZO:Cs_2CO_3/QDs/p-TPD/PEDOT:PSS/Al): (a) whole device and (b) close-up of the QD/AZO:Cs_2CO_3 interface.

clearly affected by the addition of surfactant. When PTE is not added, the current flow varies considerably from one device to another on the same substrate (almost 1 order of magnitude for low voltages), whereas when 0.5% PTE is added, the characteristics are almost identical for every point. The same observation can be made for Figure 3c,d. In the case of PEDOT:PSS with 0% PTE, the DI based PEDOT:PSS solution displays very poor wetting on the hydrophobic p-TPD layer. By

dx.doi.org/10.1021/am404876p | ACS Appl. Mater. Interfaces 2014, 6, 2508–2515

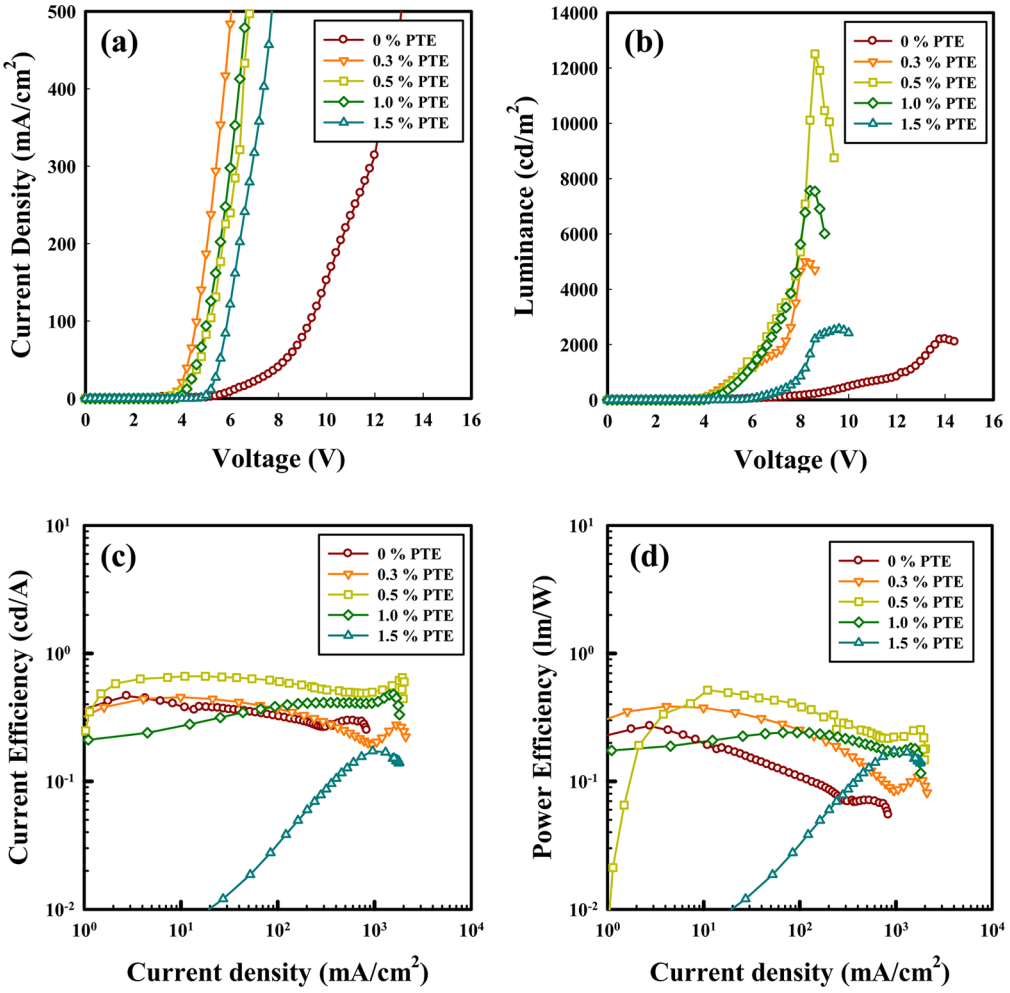

Figure 6. (a) Current density–voltage, (b) luminance–voltage, (c) current efficiency–current density (in log scale), and (d) power efficiency–current density (in log scale) characteristics for red-emitting devices with various PTE concentrations in PEDOT:PSS.

Table 2. Device Characteristics of All-Solution-Processed Red-Emitting Inverted QLEDs with Various PTE Concentrations in PEDOT:PSS

			maximum		
PTE concentration in PEDOT:PSS (%)	V_T (V)	V_D (V)	luminance (cd/m^2)	CE (cd/A)	PE (lm/W)
0	4.3	7.4	2194	0.47	0.27
0.3	2.5	4.0	5009	0.46	0.39
0.5	2.8	4.1	12 510	0.69	0.52
1.0	3.4	4.5	7566	0.48	0.24
1.5	4.9	6.3	2568	0.17	0.06

Table 3. Device Characteristics of the Red, Green, and Blue QLEDs with an Inverted Structure Fabricated by Solution Process

			maximum		
color of the QLED	V_T (V)	V_D (V)	luminance (cd/m^2)	CE (cd/A)	PE (lm/W)
red	2.8	4.1	12 510	0.69	0.52
green	3.6	4.9	32 370	2.81	1.08
blue	3.6	5.7	249	0.06	0.04

blending a surfactant in small proportions with the PEDOT:PSS solution, we are able to reduce the surface tension of the solution and therefore improve wetting on the p-TPD layer. This leads to better uniformity of the layer[23] and also better control of its thickness.

The atomic force microscopy (AFM) images and data of PEDOT:PSS surfaces with various PTE concentrations are displayed in Figure S2 and Table S1 in the Supporting Information, respectively. The improved uniformity of the current flow in the HODs indicated that the uniformity of the p-TPD/PEDOT:PSS interface is improved by adding PTE to the PEDOT:PSS solution.

However, it should be noted that there is a clear dependency of the current flow through the HODs with PTE concentration. Figure 4 shows the log current–voltage characteristics in log scale of the four HODs. A clear decrease in current flow with increasing PTE concentration can be observed, with a decrease at low voltages of more than 1 order of magnitude when going from 0 to 1.5% PTE. Since the boiling point of PTE is higher than 150 °C and the annealing temperature of the PEDOT:PSS layer is 160 °C, there is a high probability that the PTE stays in the layer after thermal annealing.

The PTE molecules at the p-TPD/PEDOT:PSS and PEDOT:PSS/Al interfaces could be responsible for blocking current through the device.[22] Note that PTE has been demonstrated to be a hole blocking material.[23]

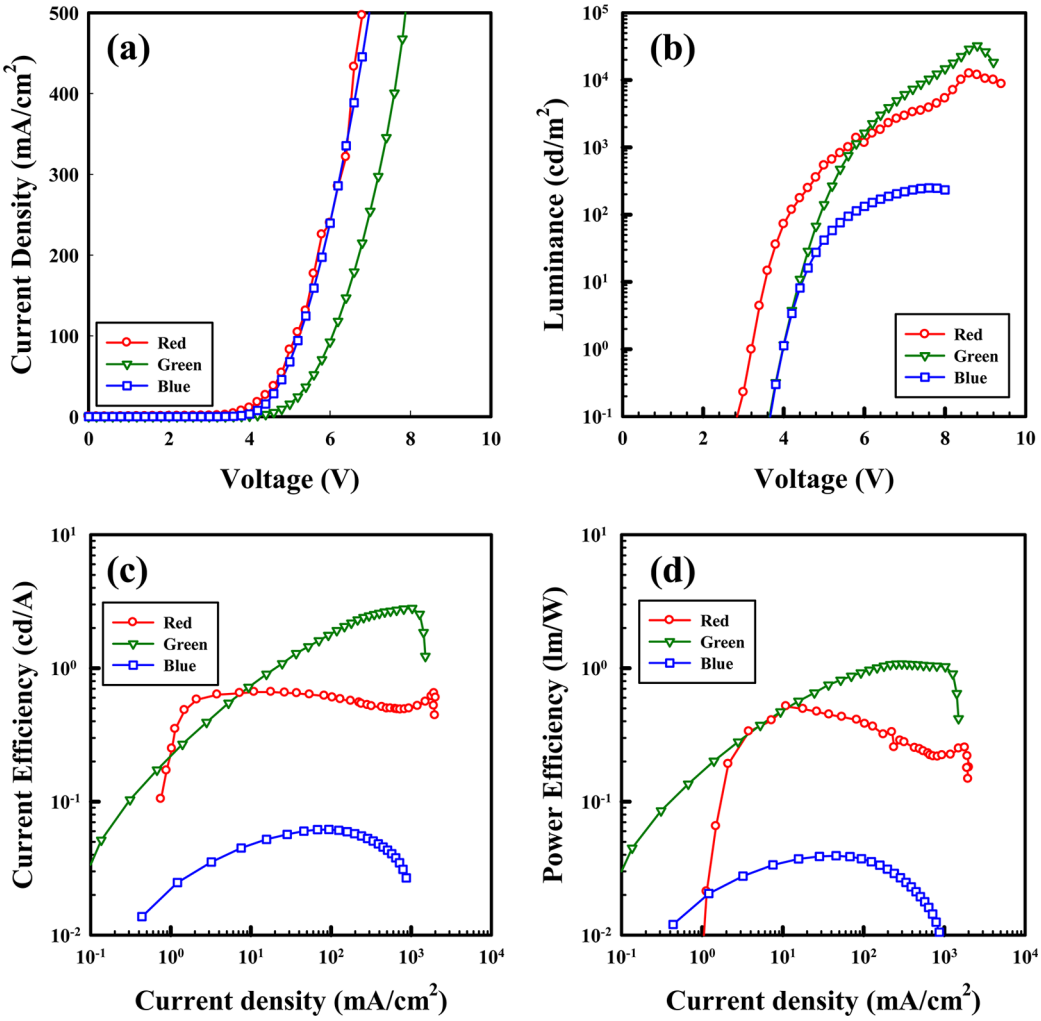

Figure 7. (a) Current density−voltage, (b) luminance (in log scale)−voltage, (c) current efficiency−current density (in log scale), and (d) power efficiency−current density (in log scale) characteristics for the red, green, and blue all-solution-processed inverted QLEDs.

Adding PTE in the PEDOT:PSS solution improves wetting on the p-TPD surface, and uniformity of the layer, but it also has the effect of decreasing current flow through the device. Therefore, the PTE content in the HIL should be carefully chosen to balance these two phenomena. According to Figure 3 and Table 1, it appears that a concentration of 0.5% PTE in the HIL solution is sufficient to ensure good wetting on the p-TPD substrate and good uniformity of current flow throughout the device compared with 0%, while allowing higher current flow than 1.0% or 1.5%.

Figure 5a shows a cross-sectional transmission electron microscopy (TEM) image of the whole inverted QLED (using red QDs for the EML), and Figure 5b shows a close-up of the QD layer and its interface with the AZO:Cs_2CO_3 layer. Figure 5a shows the multilayer structure of the device with the ITO, the AZO:Cs_2CO_3 thin film as the ETL (∼40 nm), the red QDs as the EML (2.0−2.5 MLs), a ∼70 nm thick organic layer comprising the p-TPD HTL and the PEDOT:PSS HIL with assumed thicknesses of ∼25 and ∼45 nm, respectively, and the Al anode (∼100 nm). The QDs are visible in Figure 5b; their size can be approximated to 7−8 nm.

Figure 6 shows the device characteristics of the red-emitting QLEDs with various PTE concentrations in the PEDOT:PSS films. The performance data for these devices is given in Table 2. We defined the turn-on voltage to be the applied voltage when the luminance is detected at 0.1 cd/m^2. The highest luminance was obtained for the device with 0.5% PTE in the HIL solution, with a value of 12 510 cd/m^2 compared with 2194, 5009, 7566, and 2568 cd/m^2 for 0, 0.3%, 1.0%, and 1.5% PTE, respectively. When PTE was doped into PEDOT:PSS at 0.5% concentration, device performances such as turn-on and driving voltages were improved. A clear dependency of device performance with PTE concentration can be observed in the data shown both in Table 2 and Figure 6. Comparing the device containing no PTE and the device with 0.5% PTE in the PEDOT:PSS layer, we can notice a drastic increase in performance with, for instance, maximum luminance increasing 5-fold and a 1.5 V decrease of the turn-on voltage. Then, when the devices containing PTE are compared, there is a clear increase in operating voltage of the devices and decrease in maximum luminance and current and power efficiencies with increasing PTE concentration higher than 0.5%.

The observed increase in operating voltages confirms the trend that was pointed out earlier with the study of the HODs. The efficiency of the hole injection to the EML clearly depends on the PTE concentration in the device. The increase in turn-on and driving voltages with increasing PTE concentrations in the PEDOT:PSS layer can be linked to the blocking of the current flow at the HTL/HIL and HIL/anode interfaces. As the PTE concentration increases, PTE molecules are present in

dx.doi.org/10.1021/am404876p | ACS Appl. Mater. Interfaces 2014, 6, 2508−2515

increasing numbers at these interfaces, resulting in a decrease of the efficiency of the hole injection.

It should be noted that adding even a small percentage by volume of PTE to the PEDOT:PSS solution leads to very high contents of PTE in the resulting thin film. The solid content in the initial PEDOT:PSS DI water based dispersion is 1.3−1.7% (http://www.heraeus-clevios.com). Assuming that all the water has evaporated and all the PTE stays in the layer after annealing, adding only 1% by volume of PTE to the solution would make the PTE weight percent in the layer amount to approximately 40%.[24] For this reason, PEDOT:PSS may not even represent the majority of the HIL for the device using the 1.5% PTE solution. The very high content of PTE in the layer may account for the fact that brightness and efficiency of the devices decrease considerably with increasing PTE concentrations. The increase in efficiency of the device from 0 to 0.5% PTE could be attributed to the fact that a small amount of PTE in PEDOT:PSS makes formation of PEDOT:PSS uniform on the p-TPD layer. As a result, uniform coverage of PEDOT:PSS on p-TPD can make efficient hole injection and transport to QD layer from Al. On the other hand, a large amount of PTE in PEDOT:PSS can decrease the conductivity of PEDOT:PSS because of its insulating property. Therefore, the results show that adding a small amount of surfactant in the PEDOT:PSS is necessary to ensure good device performance, and in the case of the devices fabricated in this study, the optimized concentration of PTE is 0.5%.

The performance of the red, green, and blue QLEDs all using the same multilayered structure with 0.5% PTE in the PEDOT:PSS solution is summarized in Table 3, and the characteristics of the devices are shown in Figure 7. The maximum luminances reached 12 510, 32 370, and 249 cd/m^2, and the turn-on voltages were 2.8, 3.6, and 3.6 V for the red, green, and blue devices, respectively. The three devices showed almost saturated colors with average CIE (NTSC) coordinates of (0.69, 0.31), (0.27, 0.71), and (0.18, 0.07) for red, green, and blue, respectively, as shown in Figure S3 in the Supporting Information. The color gamut expressed by the red, green, and blue QLEDs represents 147% of the NTSC 1987 color gamut. This shows one of the advantages of QLEDs for display applications.

Also Figure S4, Supporting Information, shows an external quantum efficiency (EQE) data of the red and green QLEDs with an inverted structure. It was plotted as a function of current density, and maximum EQE values of red and green QLEDs were 1.30% and 0. 88%, respectively.

4. CONCLUSIONS

In conclusion, we demonstrated the effect of PTE in the PEDOT:PSS HIL and optimized the concentration to improve the uniformity while ensuring efficient hole injection and charge balance in the device. The optimized PTE concentration in the PEDOT:PSS solution was found to be 0.5% by volume. The red, green, and blue devices using this concentration showed maximum luminances of 12 510, 32 370, and 249 cd/m^2 and turn-on voltages of 2.8, 3.6, and 3.6 V, respectively. The performances of the devices presented in this experiment do not yet match best performances reported in other studies for red inverted QLEDs, but they are nonetheless very promising because of the process used for the fabrication of the devices.

■ ASSOCIATED CONTENT

Ⓢ Supporting Information

Absorbance spectra and normalized photoluminescence intensities for the red, green, and blue QDs, atomic force microscopy (AFM) images and data of PEDOT:PSS surfaces with various PTE concentrations, average CIE (NTSC) coordinates for red, green, and blue QLEDs, and external quantum efficiency (EQE) data of the red and green QLEDs. This material is available free of charge via the Internet at http://pubs.acs.org.

■ AUTHOR INFORMATION

Corresponding Author

*Prof. Jin Jang. E-mail: jjang@khu.ac.kr. Tel: +82-2-961-0688. Fax: +82-2-961-9154.

Notes

The authors declare no competing financial interest.

■ ACKNOWLEDGMENTS

This work was supported by the Human Resources Development program (Grant No. 20134010200490) of the Korea Institute of Energy Technology Evaluation and Planning (KETEP) grant funded by the Korea government Ministry of Trade, Industry and Energy.

■ REFERENCES

(1) Wood, V.; Bulovic, V. *Nano Rev.* **2010**, *1*, 5202−5208.
(2) Shirasaki, Y.; Supran, G. J.; Bawendi, M. G.; Bulović, V. *Nat. Photonics* **2013**, *7*, 13−23.
(3) Chen, S. Y.; Chu, T. Y.; Chen, J. F.; Su, C. Y.; Chen, C. H. *Appl. Phys. Lett.* **2006**, *89*, No. 053518.
(4) Kim, H. M.; Youn, J. H.; Seo, G. J.; Jang, J. *J. Mater. Chem. C* **2013**, *1*, 1567−1573.
(5) Kwak, J. H.; Bae, W. K.; Lee, D. G.; Park, I. S.; Lim, J. H.; Park, M. J.; Cho, H. D.; Woo, H. J.; Yoon, D. Y.; Char, K. H.; Lee, S. H.; Lee, C. H. *Nano Lett.* **2012**, *12*, 2362−2366.
(6) Mashford, B. S.; Stevenson, M.; Popovic, Z.; Hamilton, C.; Zhou, Z.; Breen, C.; Steckel, J.; Bulovic, V.; Bawendi, M.; Coe-Sullivan, S.; Kazlas, P. T. *Nat. Photonics* **2013**, *7*, 407−412.
(7) Kim, L.; Anikeeva, P. O.; Coe-Sullivan, S. A.; Steckel, J. S.; Bawendi, M. G.; Bulović, V. *Nano Lett.* **2008**, *8*, 4513−4517.
(8) Haverinen, H. M.; Myllylä, R. A.; Jabbour, G. E. *Appl. Phys. Lett.* **2009**, *94*, No. 073108.
(9) Kim, T. H.; Cho, K. S.; Lee, E. K.; Lee, S. J.; Chae, J. S.; Kim, J. W.; Kim, D. H.; Kwon, J. Y.; Amaratunga, G.; Lee, S. Y.; Choi, B. L.; Kuk, Y.; Kim, J. M.; Kim, K. N. *Nat. Photonics* **2011**, *5*, 176−182.
(10) Coe-Sullivan, S. A.; Steckel, J. S.; Woo, W. K.; Bawendi, M. G.; Bulović, V. *Adv. Funct. Mater.* **2005**, *15*, 1117−1124.
(11) Huang, F.; Cheng, Y. J.; Zhang, Y.; Liu, M. S.; Jen, A. K. Y. *J. Mater. Chem.* **2008**, *18*, 4495−4509.
(12) Matyba, P.; Yamaguchi, H.; Eda, G.; Chhowalla, M.; Edman, L.; Robinson, N. D. *ACS Nano* **2010**, *4*, 637−642.
(13) Taylor, P. G.; Lee, J. K.; Zakhidov, A. A.; Chatzichristidi, M.; Fong, H. H.; DeFranco, J. A.; Malliaras, G. G.; Ober, C. K. *Adv. Mater.* **2009**, *21*, 2314−2317.
(14) Zhong, C.; Duan, C.; Huang, F.; Wu, H.; Cao, Y. *Chem. Mater.* **2011**, *23*, 326−340.
(15) Hu, W.; Henderson, R.; Zhang, Y.; You, G.; Wei, L.; Bai, Y.; Wang, J.; Wu, J. *Nanotechnology* **2012**, *23*, No. 375202.
(16) Qian, L.; Zheng, Y.; Xue, J.; Holloway, P. H. *Nat. Photonics* **2011**, *5*, 543−548.
(17) Nguyen, H. T.; Nguyen, N. D.; Lee, S. *Nanotechnology* **2013**, *24*, No. 115201.
(18) Son, D. I.; Kim, H. H.; Hwang, D. K.; Kwon, S. N.; Choi, W. K. *J. Mater. Chem. C* **2014**, *2*, 510−514.

(19) Cai, Y.; Wei, H. X.; Li, J.; Bao, Q. Y.; Zhao, X.; Lee, S. T.; Li, Y. Q.; Tang, J. X. *Appl. Phys. Lett.* **2011**, *98*, No. 113304.
(20) Park, M. H.; Li, J. H.; Kumar, A.; Li, G.; Yang, Y. *Adv. Funct. Mater.* **2009**, *19*, 1241−1246.
(21) Kim, H. M.; Yusoff, A. R. M.; Youn, J. H.; Jang, J. *J. Mater. Chem. C* **2013**, *1*, 3924−3930.
(22) Park, B.; Huh, Y. H.; Kim, M. *J. Mater. Chem.* **2010**, *20*, 10862−10868.
(23) Lee, Y. I.; Kim, M.; Huh, Y. H.; Lim, J. S.; Yoon, S. C.; Park, B. *Sol. Energy Mater. Sol. Cells* **2010**, *94*, 1152−1156.
(24) Kirchmeyer, S.; Reuter, K. J. *Mater. Chem.* **2005**, *15*, 2077−2088.